Distribution of NO_2 relative length concentration near a large industrial center

S.F. Balandin

Institute of Atmospheric Optics,
Siberian Branch of the Russian Academy of Sciences, Tomsk

Received December 28, 2004

Data of remote (up to 3 km) measurements of NO_2 profiles in a strongly polluted atmosphere of industrial center of Tomsk city are presented, obtained with the use of designed correlation spectral device DAN-2 operating with reflected and scattered solar radiation at $\lambda = 0.4$ μm. A possibility of using the scattered solar radiation reflected from different surfaces, characteristic of urban landscapes (walls and roofs of buildings, plant chimneys, trees, etc.) as a reference calibrating signal for the device has been studied. The efficiency of using such calibrating signals and calibrating signals from the background solar radiation scattered in atmosphere was compared. It was found that diffusively scattering rough underlying surfaces are most efficient for calibration of the instrument. A possibility of the device operating and measuring concentrations, integral over the path, under conditions of heavy cloudiness has been demonstrated. Mean stationary NO_2 concentration was found to be 1–5 mg/m^3 at the emission height within 100–200 m from the source and to depend weekly on the wind direction.

Recent years, correlation spectroscopy methods are considered as the most promising in designing instruments for air pollution measurements, control for engineering processes, and monitoring industrial emissions.[1–6,9–19] The technique, using a reference cell filled with some investigated impurity gas, is of the most practical interest due to its comparative simplicity.[5,8,9,13–15] Such technique was realized in the DAN-2 measuring device for visible and UV wavelengths.[2]

The block-scheme of the designed correlation analyzer[1] is presented in Fig. 1.

Radiation from sky (the diffused background), sun, or man-made source *1* passes through the cloud of the measured gas *2* to the Cassegrain telescope *4* with a big mirror of 270 mm in diameter. Then the radiation is focused by the quartz lens *5* to the diaphragm *6*, whose diameter determines the device spatial resolution. The quartz lens *7* forms a parallel light beam from the diaphragm *6*, passing through the band interference filter *8* and a calibrating quartz cell with the sensed gas fixed inside the holder *9*, which is rotated by the stepper motor *15*. Further, the light beam is divided into two channels by the semitransparent quartz plate *10* and the mirror *12*. After passing the plate *10*, the light beam through one of the channel falls on the photodetector cell *11*.

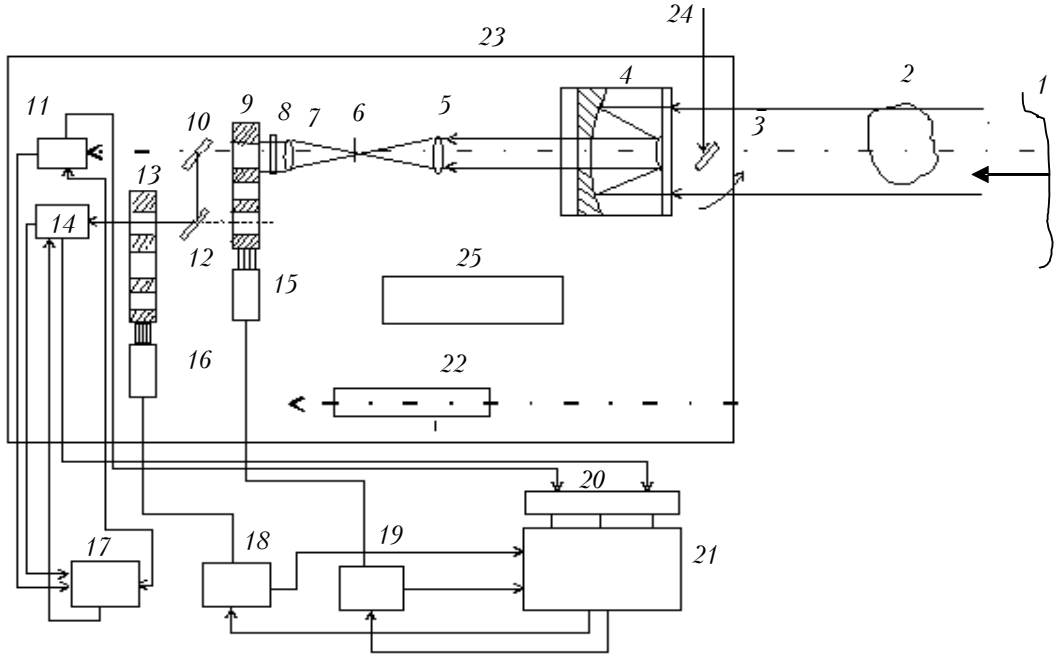

Fig. 1. The remote gas analyzer DAN-2.

0235-6880/05/11 902-08 $02.00

Through another channel, reflected by the mirror *12*, light passes the reference cell filled with the investigated gas and falls on the photodetector *14*. The reference cell is fixed inside the holder *13* rotated by the stepper motor *16*. The electronic module *17* is used both for power supply of the photodetectors *11* and *14* and for preprocessing of signals coming from them (preliminary setting of parameters). Signals from photodetectors *11* and *14* enter to the AD converter *20*, where they are quantized and enter the computer *21*. Modules *18* and *19* controlling the stepper motor produce clock signals according to the computer program.

For the analyzer pre-tuning and adjustment, the theodolite *22* is used, whose optical axis is parallel to the optical axis of the telescope *4*. The diffusive-opaque screen *3* is used for the device calibration against the sky background, the sun, or the man-made source *24*. The videocamera *25* provides for chimney plumes visualization and accurate positioning of sensing sites by characteristic topographic points. All optical system is fixed on the coordinate platform *23*, which allows a space scanning by two angular coordinates.

A real-time control for the measuring, signal processing, and display imaging is used. Automatic scanning with holders *9* and *13* favors a faster system operation and enlarges the number of components detectable for a measurement cycle. The mean measuring time does not exceed 1 min including the time for calibration of a gas component. Spatial resolution of the telescope, 3 km distant from the measurement object, achieves 1 m. Measurements of gas concentrations along the path are carried out with the DAN-2 device[2] in the following way.

1. When directing the telescope to the background atmospheric region free of the measured impurity gas, the two channels are preliminary balanced. Signals recorded by photoamplifiers are equal: $U_1 = U_2$.

2. The calibrating quartz cell filled with the measured gas of the known concentration N_{known} is inserted into the optical channel with the help of the rotating holder *9* (Fig. 1). The ratio $\frac{U_3 - U_4}{U_3 + U_4} = k_0$ is determined, where $U_3 - U_4$ is unbalance between channels U_3 and U_4 and k_0 is the calibration coefficient. On completion of the operation, the calibrating cell is removed.

3. The telescope optical axis is directed to the atmospheric region with the measured impurity gas and the ratio $\frac{U_5 - U_6}{U_5 + U_6} = k_1$ is determined, where $U_5 - U_6$ is the unbalance between received signals in case of the gas presence on the path.

4. The measured concentration of the impurity gas $\tilde{N}_x$ along the path is found from the proportion

$$\begin{matrix} k_0 - N_{\text{known}} \\ k_1 - \tilde{N}_x, \end{matrix}$$

wherefrom $\tilde{N}_x = \frac{k_1 N_{\text{known}}}{k_0}$.

In case of nonlinear dependence $k_0(N_{\text{known}})$, several k_0 values are determined for the known concentrations of the impurity gas in calibrating cells at the telescope orientation to some background free of the impurity gas. For NO_2, calibrating cells with the gas of known concentrations within the 100–2000 mg/m^2 range were used (so called length concentration accounting for the cell length). The dependence $k_0(N_{\text{known}})$ is plotted. In the absence of the calibrating cell, the telescope is directed to the atmospheric region with the measured gas and k_1 is determined. The length concentration of the gas under study, corresponding to the measured k_1, is found from the dependence $k_0(N_{\text{known}})$.

The above measurement technique is applicable only provided the spectrum of the illumination source is invariable. Its variations during path measurements can introduce additional errors.

To interpret the results of the path measurements, a possibility of the DAN-2 calibration for the conditions characteristic for *in situ* measurements have been preliminary analyzed. The transform equations of optical radiation intensity in reference and measuring channels for the pure atmosphere containing the measured impurity gas are presented in Refs. 14–17. In this work, we use these equations in the simplified form:

$$\begin{cases} I_1 = \frac{1}{\Delta\lambda}\int\limits_{\lambda_1}^{\lambda_2} C_1(\lambda) I_0(\lambda) \exp[-\tau_x(\lambda) - \tau_{\text{ref}}(\lambda)]\, \mathrm{d}\lambda \\ I_2 = \frac{1}{\Delta\lambda}\int\limits_{\lambda_1}^{\lambda_2} C_2(\lambda) I_0(\lambda) \exp[-\tau_x(\lambda)]\, \mathrm{d}\lambda, \end{cases} \quad (1)$$

where $I_0(\lambda)$ is the spectral intensity of the source radiation; I_1 and I_2 are the signals recorded in two channels; $C_1(\lambda)$ and $C_2(\lambda)$ are spectral coefficients as functions of channel transmissions within the chosen wave range $\Delta\lambda$ and chosen parameters of photodetectors; $\tau_x(\lambda)$ and $\tau_{\text{ref}}(\lambda)$ are spectral dependences of the measured gas optical thicknesses in atmosphere and the reference cell.

The value of

$$\Gamma = I_1 - I_2 / I_1 + I_2 \quad (2)$$

is displayed as a measured parameter characterizing the quantity of the absorbing mass, i.e., integral along the path concentration of the gas under study.

Let $C_1(\lambda) = C_1$, $C_2(\lambda) = C_2$, since $C_1(\lambda) = C_2(\lambda)$ within the band $\Delta\lambda$ in most practical cases.

First, to simplify the problem, set $I_0(\lambda) = \text{const}$ within $\Delta\lambda$. Under fulfillment of the channel calibration condition[2,15]

$$I_1 - I_2 = 0, \quad (3)$$

the following relation is obtained from Eq. (2)

$$C_1 < e^{-\tau_{ref}} >_{\Delta\lambda} = C_2. \quad (4)$$

It follows from Eq. (4) that the channel calibration condition (3) is defined only by the device parameters and does not depend on the scattered signal intensity I_0.

In case of the measured gas presence in the measurement path ($\tau_x \neq 0$), the integral over path absorption of the measured gas is

$$< e^{-\tau_x(\lambda)} >_{\Delta\lambda} = \frac{C_1}{C_2}\alpha < e^{-\tau_{ref}(\lambda)} >_{\Delta\lambda} \frac{[1-\Gamma]}{[\Gamma+1]} \quad (5)$$

and, as follows from Eq. (5), does not depend on I_0. Here

$$\alpha = < e^{-\tau_x(\lambda)-\tau_{ref}(\lambda)} >_{\Delta\lambda} / < e^{-\tau_{ref}} >_{\Delta\lambda}. \quad (6)$$

The left-hand side of Eq. (5) can be presented as

$$< e^{-\tau_x(\lambda)} >_{\Delta\lambda} = \exp(-\tilde{\sigma}_x \tilde{N}_{x\,abs}), \quad (7)$$

where $\tilde{\sigma}_x$ is the $\Delta\lambda$-averaged absorption cross section of the measured gas; $\tilde{N}_{x\,abs}$ is the length concentration of this gas, which can be written as

$$\tilde{N}_{x\,abs} = \tilde{N}_x \tilde{L}_x, \quad (8)$$

where $\tilde{N}_x$ is the measurement path-averaged gas concentration and $\tilde{L}_x$ is the path length. Such a presentation allows one to obtain the following $\tilde{N}_{x\,abs}$ estimation from Eqs. (6)–(8):

$$\tilde{N}_{x\,abs} = 1/\tilde{\sigma}_x \left\{ < e^{-\tau_{ref}(\lambda)} >_{\Delta\lambda} - \ln\left[\frac{C_1}{C_2}\alpha\frac{[1-\Gamma]}{[\Gamma+1]}\right]\right\}. \quad (9)$$

For typical[6,14] parameters

$$< e^{-\tau_{ref}(\lambda)} >_{\Delta\lambda} = 0.4; \ \tilde{\sigma}_x = 10^{-18}\ cm^2;$$
$$\alpha = 0.5; \ C_1 = C_2; \ \Gamma = 0.01,$$

we obtain $\tilde{N}_{x\,abs} = 5.7 \cdot 10^{18}\ cm^{-2}$, which can be realized at $\tilde{L}_x = 5 \cdot 10^4$ cm and $\tilde{N}_x = 10^{14}\ cm^{-3}$, corresponding to the NO_2 volume density of about 7 mg/m^3.

In the case of the wavelength dependence of the scattered signal intensity, the following equation can be obtained from Eq. (1) under the calibration condition (3):

$$\alpha < I_0'(\lambda) C_1 e^{-\tau_{ref}(\lambda)} >_{\Delta\lambda} - < C_2 I_0'(\lambda) >_{\Delta\lambda} = 0, \quad (10)$$

where the prime points to the wavelength dependence of the intensity. Then the calibration condition (3) can be written as

$$C_1\alpha \int_{\lambda_1}^{\lambda_2} I_0'(\lambda) e^{-\tau_{ref}(\lambda)} d\lambda = C_2 \int_{\lambda_1}^{\lambda_2} I_0'(\lambda) d\lambda. \quad (11)$$

In the presence of the background measured gas of the optical thickness $\tau_{bx}(\lambda)$ on the calibration path, the calibration condition (11) is transformed into

$$C_1\alpha \int_{\lambda_1}^{\lambda_2} I_0'(\lambda) e^{-\tau_{ref}(\lambda)} e^{-\tau_{bx}(\lambda)} d\lambda = C_2 \int_{\lambda_1}^{\lambda_2} I_0'(\lambda) e^{-\tau_{bx}(\lambda)} d\lambda. \quad (12)$$

It follows from Eqs. (11) and (12) that the measured calibration factor depends on behavior of the $I_0'(\lambda)$ function, which can be related with varying spectral background of sky or depend on the type of the underlying surface, which serves for the device calibration. Besides, the above analysis shows that the signal measured on another path can be larger or less then that corresponding to the calibration level. However, if at least one of the maxima $\lambda_{I_{max}}$ in the received signal spectrum with the half-width $\Delta\lambda_{I_{max}}$ is present in the spectral interval of the device's band-pass filter $\Delta\lambda_f$, then the measured integral concentration does not depend on the illumination background provided that $\Delta\lambda_{I_{max}} \gg \Delta\lambda_f$ and a coincidence of maxima of the filter transmissivity and the wavelength characteristic of the detected radiation. This condition is true for a number of natural objects; maxima in their spectra depend on the color temperature.

Some color temperatures[7,20–23] characteristic of the sun, blue sky, cloudiness, and moon are systematized and tabulated below along with $\lambda_{I_{max}}$ maxima in their radiation spectra.

Color temperatures for different sunlight conditions

Natural light source	$\lambda_{I_{max}}$, μm	Color temperature, T, K
Morning or evening twilight sky	1.70	2000
Sky nearby rising or setting sun	1.30	2300–2400
Sun in an hour after rise	0.90	3500
Sun an hour before set	0.90	3500
Moon	0.75	4125
Morning or evening sun in a clear sky at an angle more than 15° above the horizon	0.90–0.70	3600–5000
Noon sunlight at thin clouds	0.70–0.60	5100–5600
Summer noon sunlight in clear blue sky near the Earth surface	0.70–0.60	5300–5700
Noon sunlight at thin clouds	0.50–0.60	5700–5900
Zenith summer sun in clear blue sky	0.50–0.48	6000–6500
Day sunlight at high thin clouds	0.49–0.48	6700–7000
Day sunlight at thick clouds	0.49–0.43	7000–8500
Day sunlight at thin clouds	0.35–0.30	12000–14000
Cloudy sky in the northern part	0.35–0.12	12000–25000
Clear blue sky	0.20–0.10	15000–27000

The data show the maximum of spectral intensity to shift from the blue (clear blue sky) to red (sunrise or sunset) regions. The sky color temperature is much higher than the sun's one both under thick and, especially under thin cloudiness (12000–14000 K). Thus, clouds, depending on their illumination, can significantly distort the solar spectrum and influence measurement results.

Theoretically, it is impossible to consider all spectral variations registered by correlating receivers and to estimate their effect on measurement errors in integral concentrations along a sounding path. Therefore, experiments were carried out with the purposes to estimate the influence of types of reflecting surfaces and varying airglow diffuse background on the possibility to recover averaged profiles of impurity gas concentrations in atmosphere.

Figure 2 illustrates a general scheme of experiments carried out on different sounding paths in actual atmosphere using the DAN-2 device.

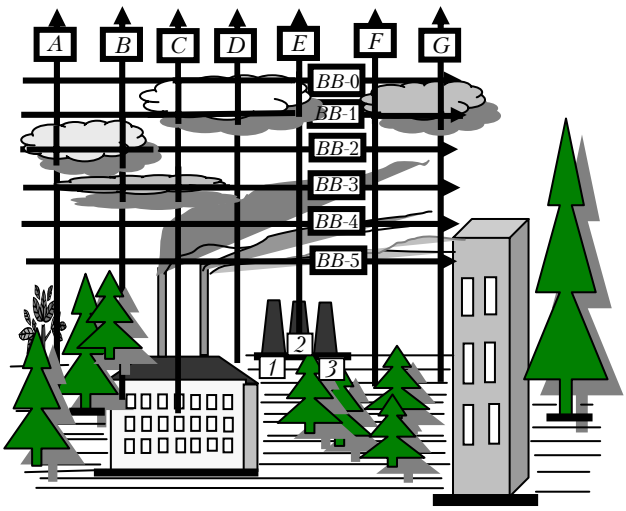

Fig. 2. General view of the terrain near some industrial enterprise in Tomsk city and sections of NO_2 measurements in atmosphere.

Numbers *1–3* correspond to cooling towers of the Tomsk electric power station (GRES-2). The *A*-section is located between trees (pine, fir) and the calibration was performed against the trees upward. The *B*-section crosses trees and a building while the *C*-section goes between plant chimneys, crossing the building and its roof. Sections *D*, *E*, and *F* either cross a cooling tower (*E*) or start from the ground surface. The *G*-section starts from the ground surface and goes close to the building. The telescope's vertical scanning field is given in relative angular units $\frac{W}{\Delta W}$, where W is the current scanning angle from the beginning of some section (upward or downward) and ΔW is the scanning angle range in a chosen section, which made ≈ 25–30° depending on the terrain landscape.

Horizontal sections in Fig. 2 are denoted as *BB*-0 – *BB*-5. The telescope scanning along these sections were carried out both from left to right and from right to left (see Fig. 4) at an angle $W = 15–25°$ from the section beginning. The distance to the observed object was about 3 km. At this distance, the Cassegrain telescope reliably received optical signals from an area of 2 m in diameter. A spatial filtration of the received radiation was performed through a diaphragm in the telescope focal plane. The initial calibration of optical signals was carried out in a calibrating cell of 5 cm in length at the NO_2 length concentration of 1000 mg/m^2. The length concentration of a measured gas was normalized to the maximum in each section.

Figure 3 presents experimental results most characteristic of vertical profiles. The vertical profile of the relative length NO_2 concentration is shown in Fig. 3*a* (section *C*) at a top-down telescope scanning and the calibration against scattered radiation of the upper sky. The characteristic minimum is connected with weak scattering of solar radiation by a dense (black) smoke; therewith, the scattering spectrum is not distorted significantly. In this case, the integral concentration along the path decreases significantly due to the gas wind drift in the sensing direction. At the same time, the integral background concentration is much higher when calibrating against the clear sky background (initial signal level) than against a chimney smoke with a much shorter distance from the telescope to the object.

Another interesting experimental result is presented in Fig. 3*b*. Here, the calibration was carried out at a fine sunny weather (section *C*). The telescope moved from the plant chimney up to the level of sky background glow (used for the device calibration in the case of the telescope top-down movement). It is evident that mean signal levels practically coincide (up to 5%) at focusing to the background and calibrating against the chimney. Hence, we can conclude that gray diffusively reflecting surfaces can be used for calibration. This result was proved by similar measurements carried out when calibrating against the surface of the incline unlit dark-red roof, dark diffusively reflecting surface of the cooling tower, and the Earth's surface.

Light buildings, green vegetation, and snow lead to ambiguous calibration.[4] This is illustrated in Fig. 3*c* (section *B* in Fig. 2). The calibration was carried out against the dark green coniferous forest (initial part of the curve), then against the light building and its dark red roof. The building and the forest were not exposed to sunshine. Calibrating signals for the roof and building quite good agree with the background level (end of the curve) while the coniferous forest-calibrating signal is 30% overestimated. In the case of exposure of trees and the building to sunshine, the level of calibrating signals sharply rose, that made measurements practically impossible. Similar situation was when calibrating from snow, since the calibrating signal exceeded that of background measurements along sections.

Studies conducted under cloudiness conditions have shown that measurements of integral concentrations and calibration of instruments are possible only against dark surface under conditions of dark and dark-gray clouds. Under light clouds (e.g., cirrus) the measurements are impossible because of their high variable brightness temperature (see Table). Most typical results for calibrating against different surfaces under clouds are shown in Fig. 3*d*. Under continuous and dark clouds (Cu, Cb), when calibrating against the building roof (Fig. 3*e*), the calibrating results practically coincide with the background concentration measured in the upper point of the vertical profile. The curve is broken due to influence of cloud optical parameters.

Light gray clouds (As, Ci, Cc) (Fig. 3*f*) do not allow the profile of concentration variations to be obtained, while the calibration (roof, chimney) is acceptable and the integral concentration level can be obtained.

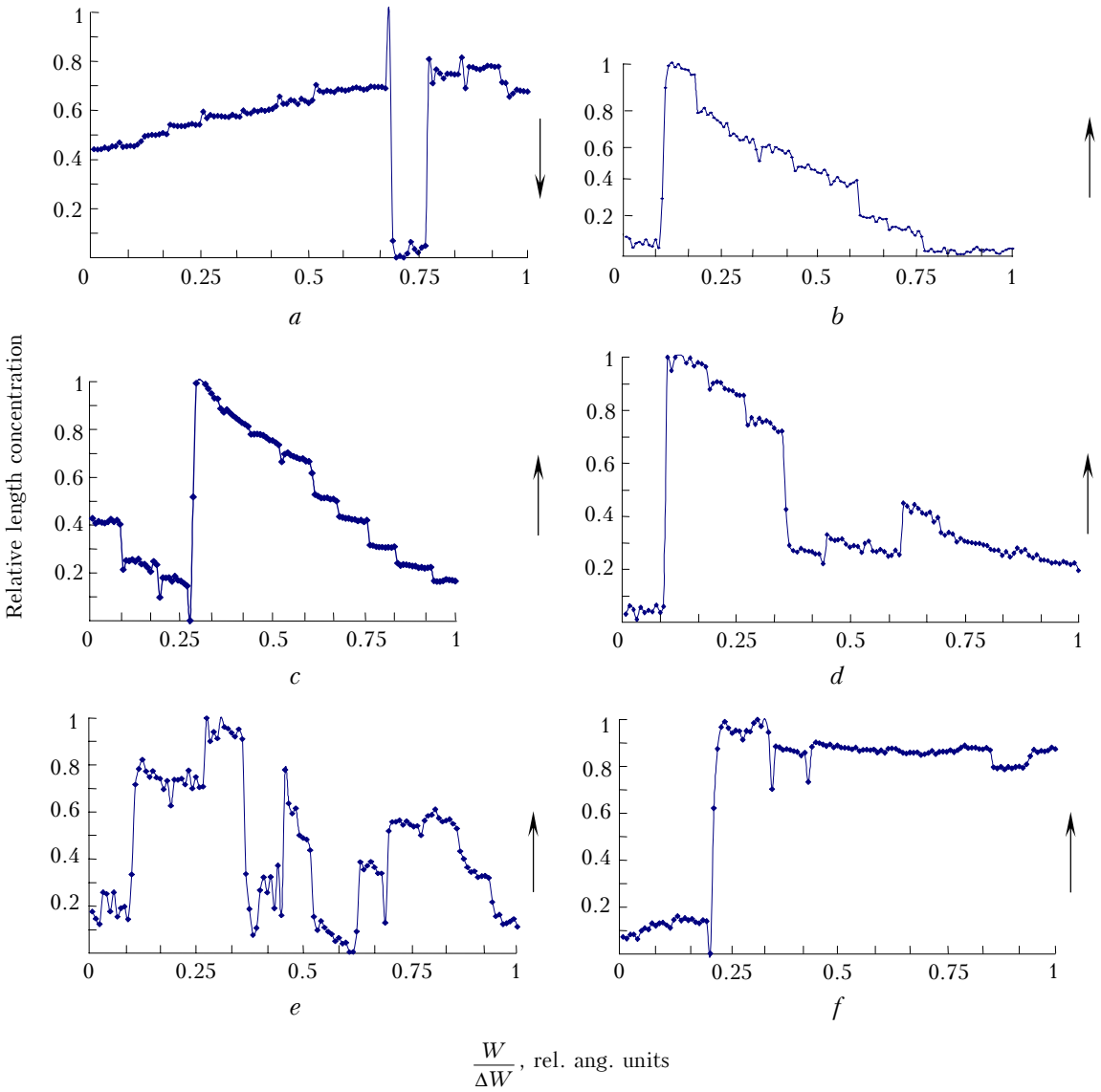

Fig. 3. Relative length NO_2 concentration at vertical sections. Arrows show the direction of movement of the telescope optical axis in the observed area: section *C*, April 14, 2003, 15:40, calibration against clear atmosphere (section top), thin and ragged clouds, east wind of 3–5 m/s (*a*); section *B*, April 8, 2003, 13:01, calibration against the GRES-2 chimney, thin and ragged clouds, north wind of 2–5 m/s (*b*); section *B*, April 18, 2003, 15:05, calibration against buildings and trees, clear atmosphere, south wind of 3–5 m/s (*c*); section *E*, April 25, 2003, 15:52, calibration against the cooling tower, continuous dark gray clouds, north wind of 3–8 m/s (*d*); section *C*, April 24, 2003, 15:15, calibration against the building roof, nonuniform dark gray clouds, north-west wind of 1–3 m/s (*e*); section *C*, May 20, 2003, 15:35, calibration against the roof and chimney, light gray clouds, southwest wind of 2–5 m/s (*f*).

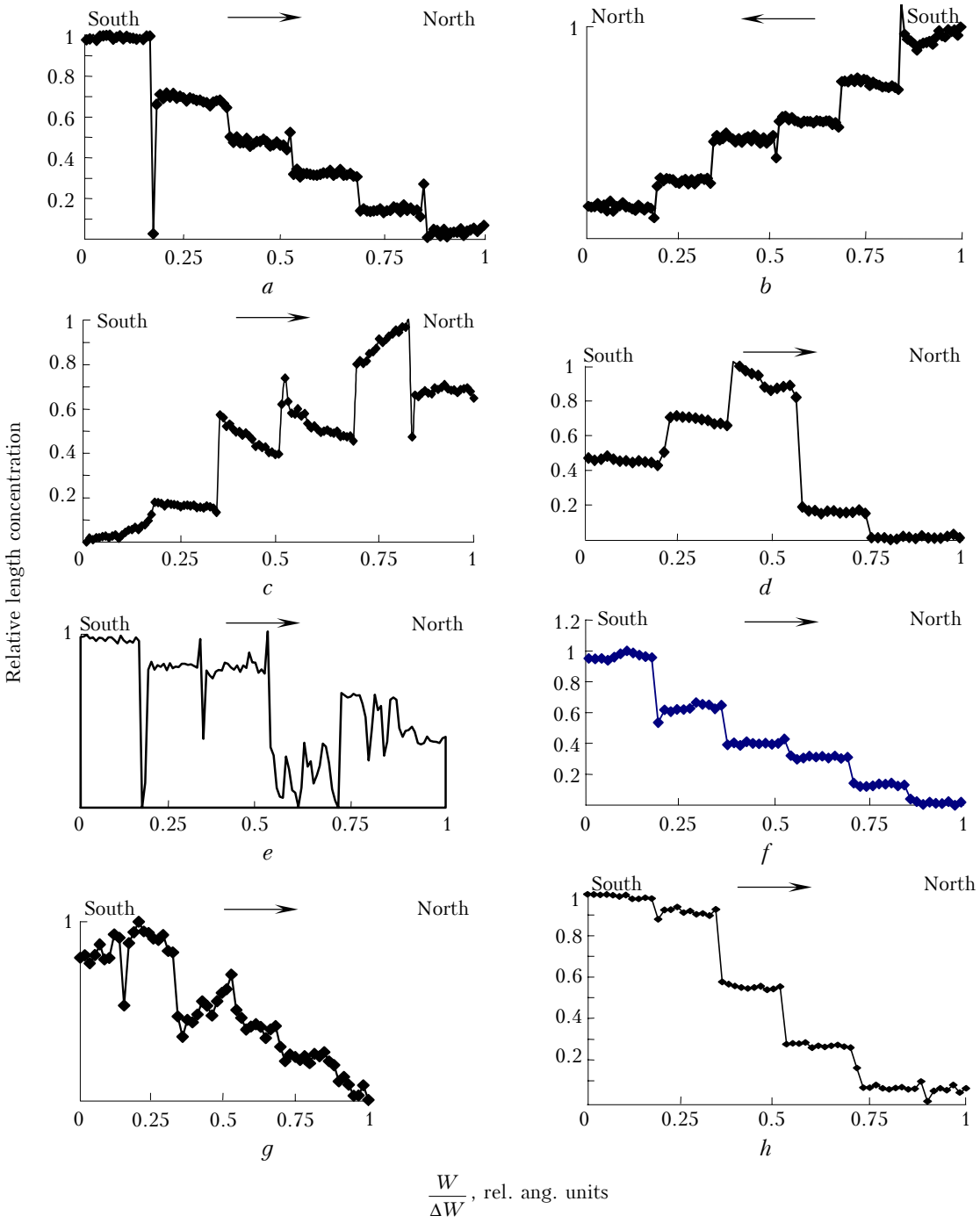

Fig. 4. Relative length NO_2 concentration for horizontal sections *BB*-1 – *BB*-5. Arrows show the direction of the telescope optical axis movement in the observation space: section *BB*-1, March 14, 2003, 14:05, clear sky, north wind of 1–3 m/s (*a*); the same conditions at 14:07 (*b*); section *BB*-3, December 10, 2002, 12:55, clear sky, south wind of 2–5 m/s (*c*); section *BB*-1, March 7, 2003, 16:40, clear sky, north wind of 2–4 m/s (*d*); section *BB*-5 (at a height of the chimney), January 27, 2003, 13:30, continuous cloudiness, northwest wind of 3–8 m/s (*e*); section *BB*-2, March 11, 2003, 16:35, thin mist (the visibility is about 5 km), north wind of 1–3 m/s (*f*); section *BB*-1, January 6, 2003, 12:45, haze (the visibility is about 4 km), north wind of 1–3 m/s (*g*); the section *BB*-5, January 30, 2003, 15:15, thin mist (visibility is about 4 km) (*h*).

Results representative for horizontal sections are shown in Fig. 4. The plots in Figs. 4*a* and *b* present curves obtained at the vertical part of the chimney plume. The sectioning was performed both in forward and backward directions of the telescope axis movement at clear weather practically in the same observational time. As is seen, under weak north wind the relative length NO_2 concentration measured

in the south direction is much higher than in the north one. Some difference (no more than 15%) between the initial and final (Figs. 4*a* and *b*) parts of the sensing path can be explained by different conditions of signal calibration in the presence of NO_2 impurity gas, because the calibration was carried out immediately in the initial and final parts of the horizontal profile *BB*-1 (see Fig. 2).

The next plot (Fig. 4*c*) shows the concentration profile of NO_2 in the *BB*-3 section under south wind and clear sky. The concentration maximum is observed in the north sensing direction. A moderate signal maximum is seen concerned with the impurity gas absorption within the sensing zone. Under north wind and clear sky the maximum shifts southward (near the chimneys) (Fig. 4*d*) are observed. In general, the total NO_2 content is higher in the south direction then in the north one. Such tendency is true for most experiments (80%) and can be explained by predominance of industrial enterprises in the southern part of Tomsk city (7 objects) as compared to its northern part (2 objects) within a 3-km radial zone of the GRES-2 chimneys.

Clear sky measurements have shown the absolute values of length concentrations along the path near the GRES-2 chimneys to fall into the 1000–2000 mg/m^2 range. A permanent gas anomaly has been found located 100–200 m radially from the emission source and at a moderate wind weakly dependent on its direction. Subtracting the background atmospheric NO_2 concentration, which is about 500 mg/m^2 for a 10-km path and a typical gas anomaly size of about 400 m, from the above moduli, we obtain an average volume concentration of 1.5–5 mg/m^3 within the gas anomaly zone. This result is in good agreement with the estimation by Eq. (9).

Measurements obtained under different weather conditions (Figs. 4*d–h*) confirm, in principle, the patterns obtained for clear weather. Thin mist, haze, and clouds are no bar for measurements providing the observed object is visible. Discontinuous signal is characteristic of cloudiness (Fig. 4*e*); however, it illustrates the tendency of concentration variation along the given section. It should be noted, that the background cloud radiation distorts the recorded signal in a lesser degree when scanning sections at low angles with respect to the horizon (Fig. 4*e*) than when scanning vertical profiles of clouds (*C*-section, Fig. 3*f*).

Conclusion

It is shown, that the highest sensitivity and the lowest error in path measurements of impurity NO_2 in the real atmosphere can be attained only provided that the maximum of spectral characteristic of a received optical signal coincides with the maximum or is essentially wider than the transmission band $\lambda = 0.38–0.42$ μm of the device's band-pass filter.

It is experimentally found that the most significant distortions in measurements of path-integral concentrations are observed under thin clouds; the presence of heavy cloudiness allows recovering of integral gas concentrations. The background effect of clouds nearby the horizon is significantly weaker at a horizontal sectioning then at vertical one. Length NO_2 concentrations in atmosphere along the chosen sections are recoverable under heavy cloudiness (dark and dark-gray clouds).

When calibrating the DAN-2 instrument against different surfaces, it is necessary to account for their illumination and reflectance. Diffusive unlit surfaces are most acceptable for the device calibration while the fine weather or heavy cloudiness – for path measurements of length concentrations.

Permanent gas anomaly has been found in a 100–200 m radial distance from the emission source, which has an average volume concentration about 1.5–5 mg/m^3 and at a moderate wind weakly depends on its direction.

References

1. S.F. Balandin, Proc. SPIE **5743**, 28–33 (2004).
2. S.F. Balandin, Yu.D. Kopytin, V.I. Kokhanov, and S.A. Shishigin, Proc. SPIE **5396**, 49–56 (2004).
3. S.F. Balandin and S.A. Shishigin, in: *Int. Conf. on Optical Technol. for Atmosph., Ocean and Environment. Studies* (ICOT) (Beijng, China, 2004), pp. 71–72.
4. S.F. Balandin, in: *XI Int. Symp. on Atmospheric and Ocean Optics. Atmospheric Phys.,* Tomsk (2004), pp. 50.
5. S.F. Balandin, Yu.D. Kopytin, S.A. Shishigin, V.I. Kokhanov, and A.I. Petrov, in: *Abstracts of Reports at VII Int. Symp. on Atmospheric and Ocean Optics,* Tomsk (2000), p. 114.
6. Yu.D. Kopytin, V.V. Nosov, A.B. Antipov, A.I. Isakova, M.A. Samokhvalov, and L.K. Chistyakova, in: *Remote Techniques for Oil, Ore, and Man-caused Anomaly Forecast by Geoatmospheric Manifestations* (Publishing House of IAO SB RAS, Tomsk, 2000), pp. 99–103.
7. M.V. Kabanov and M.V. Panchenko, in: *Optical Wave Scattering by Disperse Media.* Part 3. *Atmospheric Aerosol* (Publishing House of the Tomsk Branch of SB AS SSSR, Tomsk, 1984), pp. 142–153.
8. S.F. Balandin, Izv. Vyssh. Uchebn. Zaved. Fiz., No. 3, 95 (2000). Dep. VINITI, reg. No. 3521-1399 of 29.11.99. 30 pp.
9. S.F. Balandin, Yu.D. Kopytin, V.I. Kokhanov, S.A. Shishigin, and A.I. Petrov, in: *Abstracts of Reports at VI Int. Symp. on Atmospheric and Ocean Optics,* Tomsk (1999), pp. 117.
10. S.F. Balandin, Yu.D. Kopytin, V.I. Kokhanov, and S.A. Shishigin, in: *X Workshop on Siberian Aerosols,* Tomsk (2003).
11. S.F. Balandin, Yu.D. Kopytin, V.I. Kokhanov, and S.A. Shishigin, in: *Abstracts of Reports of Joint Int. Symp. on Atmospheric and Ocean Optics,* Irkutsk (2001), p. 156.
12. S.F. Balandin, Yu.D. Kopytin, and V.I. Kokhanov, in: *Abstracts of Reports of Joint Int. Symp. on Atmospheric and Ocean Optics,* Irkutsk (2001), p. 156.
13. B.T. Tolton, J. Atmos. Ocean Technol. **21**, 837–852 (2004).
14. H.S. Lee and H.H. Zwick, Pribory Nauch. Issled., No. 9, 132–149 (1985).
15. B.T. Tolton and D. Plouffe, Appl. Opt. **40**, 1305–1313 (2001).

16. R.M. Richard, J. Opt. Soc. Am. **58**, No. 7, 900–908 (1968).
17. T.V. Ward and H.H. Zwick, Appl. Opt. **14**, No. 12, 2896–2904 (1975).
18. M.K. Shaikov, E.A. Chayanova, and E.V. Ivanov, Atm. Opt. **3**, No. 3, 285–288 (1990).
19. E.A. Chayanova and M.K. Shaikov, Zh. Prikl. Spektrosk. **51**, No. 4, 639–646 (1989).
20. *ASTER* Spectral library. 2005. http://speclib. naca. gov
21. S.V. Garbuk and V.E. Gershenzon, *Space Remote Sounding Systems* (A&B Publishing House, Moscow, 1997), 206 pp.
22. V.P. Savinykh and V.A. Solomatin, *Optical-Electronic Systems of Remote Sounding* (Nedra, Moscow, 1995), 310 pp.
23. E. Shanda, *Physical Foundations for Remote Sounding* (Nedra, Moscow, 1990), 203 pp.